THE PHYSICS OF FLUIDS VOLUME 15, NUMBER 9 SEPTEMBER 1972

Radiative Transport Analysis of Electromagnetic Propagation in Isotropic Plasma Turbulence

DAVID L. FEINSTEIN,* FRANK E. BUTLER, AND KENNETH R. PIECH
Cornell Aeronautical Laboratory, Incorporated, Buffalo, New York 14221
AND
ANTHONY LEONARD
Stanford University, Stanford, California 94305

(Received 21 July 1971; final manuscript received 29 March 1972)

The problem of electromagnetic wave propagation in a turbulent plasma is formulated in terms of the radiative transport equation. A singular eigenfunction solution is obtained for the case of isotropic plasma turbulence, and detailed numerical calculations are presented. The intensity distribution is studied as a function of the turbulent spectrum and relative strength of scattering attenuation to total attenuation. For a highly forward peaked scattering law characteristic of many physical situations it is found that the reflected backscatter intensity is relatively insensitive to the angle of incidence, except as grazing incidence is approached. The importance of multiple scatter is studied as a function of the properties of the medium.

I. INTRODUCTION

In an attempt to develop a theory of electromagnetic scattering from turbulent ionized media, we have developed and reported on an analysis based on the radiative transport equation.[1] Initially, the formulation considered only the first two terms of the Neumann series solution to the scalar equation. Later, an improved physical representation was investigated by considering the Neumann series solution to the vector equation.[2] This approach has been successful in predicting the percentage depolarization for two different experimental configurations.[1,3] However, the rate of convergence of the Neumann series becomes slower when one progresses away from the Born scattering region (where the mean and fluctuating components of the electron number density must be well below the critical electron number density) and approaches overdense scattering conditions and hence, the validity of the calculation is questionable in that range. For this reason, in this paper we use an exact solution to the scalar transport equation which is not dependent upon the convergence properties of a particular series expansion.

A number of techniques are available for solving the radiative transport equation, e.g., Monte Carlo,[4] invariant imbedding,[5] discrete ordinates,[6] or singular eigenfunction expansions.[7] In this work we wish to investigate the effects of multiple scattering and of changes in the turbulence spectrum; hence, we find it sufficient to consider only simple geometries. Thus, the singular eigenfunction method, suitable for plane-parallel homogeneous media, is the method which is utilized. For the case of a homogeneous half-space, this method provides the exact solution in terms of the quadratures. The other above-mentioned techniques would require a more significant computing effort. For a complicated geometry, on the other hand, the Monte Carlo approach might be the optimum choice. In this work, we develop the necessary numerical analysis in order to proceed from the formal derivations and solutions of the radiative transport equation[8–13] to numerical results and study the scattering as a function of medium characteristics. Watson[9] has studied this problem for the case of isotropic scattering or the long wavelength limit.

In the next section we briefly review the radiative equation formalism as applied to the problem of microwave scattering from a turbulent plasma.[3,9,12,14] We also describe a computational scheme based on the singular eigenfunction solution to the transport equation for the case of an isotropic turbulence spectrum. In this case the scattering function is rotationally invariant and can be approximated by a finite series of Legendre polynomials. Scattering in a turbulent plasma can be highly anisotropic which leads to computational limitations. Other authors have considered highly anisotropic scattering but only azimuthally symmetric radiation fields.[15,16] In the third section, we present and interpret the numerical results for both the reflected intensity and the intensity distribution in the model medium. We investigate the effect of changes in the turbulence spectrum and in the relative attenuation due to scattering and adsorption. The limitations of the present approach are discussed. The final section summarizes the results and conclusions of the paper.

Before proceeding we should emphasize the difference between the terms homogeneity of the plasma medium, isotropy of the turbulence, and isotropy of the scattering function. The first, homogeneity of the plasma medium means that the statistical averages are uniform in space. The second, isotropy of the turbulence means that the turbulent spectrum is not a function of the wave vector $\mathbf{k}$ but rather just of the magnitude $|\mathbf{k}|$. The third, isotropy of the scattering function means that scattering has equal probability in all directions. In this paper we assume homogeneity of the plasma medium and isotropy

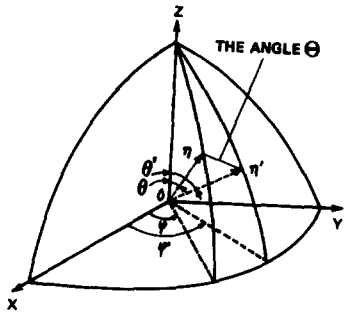

FIG. 1. Geometry for scattering through angle Θ.

of the turbulence but not the isotropy of the scattering function.

II. SOLUTION OF THE RADIATIVE TRANSPORT EQUATION FOR A LEGENDRE POLYNOMIAL FIT TO A ROTATIONALLY INVARIANT SCATTERING LAW

A. Formulation of Problem

The radiative transport equation for the intensity, $I(\mathbf{r}, n)$, (power at $\mathbf{r}$ flowing in direction n, per unit solid angle about n per unit volume at $\mathbf{r}$), in the medium is

$$(n\cdot\nabla)I(\mathbf{r}, n)+[\kappa(\mathbf{r})+\sigma(\mathbf{r})]I(\mathbf{r}, n) =[\sigma(\mathbf{r})/4\pi]\int d\Omega(n')p(n, n')I(\mathbf{r}, n'), \quad (1)$$

where we have written the scattering law in the form $\sigma(\mathbf{r})[p(n, n')/4\pi]$ with $(4\pi)^{-1}\int p(n, n')\,d\Omega(n')=1$. In Eq. (1) $\sigma(\mathbf{r})$ is scattering probability per unit length and $\kappa(\mathbf{r})$ represents absorption probability per unit length. We assume $I(\mathbf{r}, n)$ represents intensity of a given frequency, and that energy exchange between frequencies can be neglected. The quantity $d\Omega(n')$ is a differential solid angle about n'. Rigorous derivations of Eq. (1) and a discussion of the range of validity of this equation may be found in the literature.[8,9,10,13]

Our intent here is to investigate the solutions of Eq. (1) for a homogeneous half-space with a scattering law characteristic of an isotropic turbulent plasma. We thus assume the medium under consideration fills the half-space $z>0$ and, with the homogeneity assumption, write Eq. (1) in the form

$$\left(\mu\frac{\partial}{\partial x}+1\right)I^m(x, \mu)=\tfrac{1}{2}\tilde{\omega}_0\int p^m(\mu, \mu')I^m(x, \mu')\,d\mu', \quad (2)$$

where x is the optical thickness

$$x=\int_0^z(\kappa+\sigma)\,dz'=z(\kappa+\sigma), \quad (3)$$

and the single scatter albedo $\tilde{\omega}_0$ is

$$\tilde{\omega}_0=\sigma/(\kappa+\sigma). \quad (4)$$

In Eq. (2) $\mu=\cos\theta$, the cosine of the polar angle. The scattering phase function p is assumed to be azimuthally symmetric. The coordinate system is shown in Fig. 1. In general, I will depend on (x, μ, φ); hence, we have also made the usual expansions

$$I(x, \mu, \varphi)=\sum_m \exp(im\varphi)I^m(x, \mu),$$
$$p(n, n')=\sum_m \exp[im(\varphi-\varphi')]p^m(\mu, \mu').$$

Since the $\exp(im\varphi)$ form an orthogonal set, Eq. (2) holds for each m with no coupling between different values of m. Equation (2) thus represents a set of equations describing radiative transport within the model space.

B. Method of Solution

We briefly outline the singular eigenfunction solution technique as applied to Eq. (2). Since the details of the solution may be found in McCormick and Kuščer,[12] we merely sketch the important points. We first assume that the scattering phase function can be approximated by

$$\tilde{\omega}_0p(\cos\Theta)=\sum_{l=0}^{N}\tilde{\omega}_lP_l(\cos\Theta), \quad (5)$$

where Θ is the scattering angle, and P_l are the Legendre polynomials. We note that the expansion of $p(\cos\Theta)$ in Legendre polynomials is not the only possible procedure. Other basic functions could be utilized, or one could deal directly in the computations with $p(\cos\Theta)$. Use of an analytical expression for $p(\cos\Theta)$ such as Eq. (5), however, allows the formal analysis to be carried farther than in a purely numerical treatment.

Use of the ansatz

$$I^m(x, \mu)=\exp(-x/\mu)\phi^m(\nu, \mu)(1-\mu^2)^{m/2} \quad (6)$$

yields the equation for the eigenfunctions ϕ^m

$$(\nu-\mu)\phi^m(\nu, \mu)=\tfrac{1}{2}\nu\int_{-1}^{+1}p^m(\mu, \mu')\phi^m(\nu, \mu')\,dm(\mu'), \quad (7)$$

where ν plays the role of an eigenvalue, and

$$p^m(\mu, \mu')=\sum_{l=m}^{N}c_l{}^m p_l{}^m(\mu)\,p_l{}^m(\mu').$$

In the above $p_l{}^m(\mu)$ are the associated Legendre polynomials divided by $(1-\mu^2)^{m/2}$ and

$$c_l{}^m=\tilde{\omega}_l(l-m)\,!/(l+m)\,!.$$

We have also introduced the notation

$$dm(\mu)\equiv(1-\mu^2)^m d\mu.$$

The singular eigenfunction approach is similar to the standard techniques used to solve ordinary differential equations. One first seeks the solutions of eigenfunctions $\phi^m(\nu, \mu)$ of the homogeneous transport equation, Eq.

(7). The solution for I is then expanded in terms of these eigenfunctions with the expansion coefficients determined by the boundary conditions. In general, there are two types of solutions to Eq. (7): continuum solutions and discrete solutions.

(i) Continuum Solutions

For $\nu\in(-1,1)$ there corresponds a continuous set of singular eigensolutions

$$\phi^m(\nu,\mu)=\tfrac{1}{2}\nu g^m(\nu,\mu)P(\nu-\mu)^{-1}+\lambda^m(\nu)(1-\nu^2)^{-m}\delta(\nu-\mu), \quad (8)$$

where P denotes the Cauchy principal value, and

$$\lambda^m(\nu)=1-\tfrac{1}{2}\nu P\int_{-1}^{+1}\frac{g^m(\nu,\mu)\,dm(\mu)}{(\nu-\mu)}, \quad (9)$$

$$g^m(\nu,\mu)=\sum_{l=m}^{N}c_l{}^m g_l{}^m(\nu)p_l{}^m(\mu), \quad (10)$$

$$g_l{}^m(\nu)=\int_{-1}^{+1}\phi^m(\nu,\mu)p_l{}^m(\mu)\,dm(\mu). \quad (11)$$

(ii) Discrete Solutions

For $\nu\notin(-1,1)$ there may exist a set of discrete eigenfunctions

$$\phi^m(\pm\nu_j{}^m,\mu)=\tfrac{1}{2}\nu_j{}^m[g^m(\pm\nu_j{}^m,\mu)/(\nu_j{}^m\mp\mu)], \quad (12)$$

which are the roots of the dispersion relation

$$\Lambda^m(z)=0, \quad (13)$$

where $\Lambda^m(z)$ has the same integral representation as $\lambda^m(\mu)$ but with $z\notin(-1,1)$. The number of discrete roots may be found by the argument principle

$$M=\pi^{-1}[\Delta\arg\Lambda_+{}^m(\nu\pm i\epsilon)]_{0\to1}, \quad (14)$$

where M is the number of discrete roots with positive real parts and

$$\Lambda_\pm{}^m(\nu)=\lim_{\epsilon\to0^+}\Lambda^m(\nu\pm i\epsilon)=\lambda^m(\nu)\pm\tfrac{1}{2}i\pi\nu g^m(\nu,\nu)(1-\nu^2)^m. \quad (15)$$

In Eq. (14) $[\Delta\arg\Lambda_+{}^m(\mu)]_{0\to1}$ is the change in the argument of $\Lambda_+{}^m(\mu)$ as μ varies continuously from 0 to 1.

It can be shown that the number of positive roots is limited by[11]

$$M\leq N-m+1$$

with N the highest-order Legendre polynomial occurring. It can be shown that there is at least one real positive root for $m=0$.[11] As $\tilde{\omega}_0$ increases, ν_0' increases to infinity and additional roots appear at $\nu=1$. We also note, as the order of the polynomial fit is increased, that there is the possibility of additional roots.

Once the eigenfunctions Eqs. (8) and (12) have been found, it is necessary to establish the completeness of the ϕ^m, so that an expansion of I^m in terms of the ϕ^m can be properly made and interpreted. Completeness of the ϕ^m follows from a theorem[7,12] which states that an arbitrary Hölder continuous function on $[0,1]$ can be expanded in terms of the ϕ's as

$$I_m(x,\mu)=\sum_{j=1}^{M}a_j{}^m\phi^m(\nu_j{}^m,\mu)\exp(-x/\nu_j{}^m)+\int_0^{+1}A^m(\nu)\phi^m(\nu,\mu)\exp(-x/\nu)\,d\nu. \quad (16)$$

The proof is constructive in that once completeness is proven, it explicitly yields a calculational scheme for the expansion coefficients $a_j{}^m$ and $A^m(\nu)$. For details of the proof, the reader is referred to the literature.[7,12] We simply quote the results relevant to our problem.

The expansion coefficients may be written in terms of the adjoint eigensolutions as

$$a_j{}^m=\frac{\pi^{-1}\tilde{\phi}^m(\nu_j{}^m,\mu_0)\mu_0H^m(\mu_0)}{(\nu_j{}^m)^2g^m(\nu_j{}^m,\nu_j{}^m)H^m(\nu_j{}^m)[d\Lambda^m(z)/dz]\,|_{z=\nu_j{}^m}}, \quad (17)$$

$$A^m(\nu)=\frac{(2\pi)^{-1}\tilde{\phi}^m(\nu,\mu_0)H^m(\mu_0)(1-\nu^2)^m}{X^m(\nu)\nu H^m(\nu)}, \quad (18)$$

$$X^m(\nu)=\Lambda_+{}^m(\nu)\Lambda_-{}^m(\nu). \quad (19)$$

The adjoint eigensolutions are given by

$$\tilde{\phi}^m(\nu_j{}^m,\mu_0)=\tfrac{1}{2}\nu_j{}^mB^m(\nu_j{}^m,\mu_0)+\frac{\tfrac{1}{2}\nu_j{}^mg^m(\nu_j{}^m,\mu_0)}{(\nu_j{}^m-\mu_0)} \quad (20)$$

and

$$\tilde{\phi}^m(\nu,\mu_0)=\tfrac{1}{2}\nu\left[B^m(\nu,\mu_0)+\frac{g^m(\nu,\mu_0)}{(\nu-\mu_0)}\right]+\frac{\lambda^m(\nu)\delta(\nu-\mu_0)}{(1-\nu^2)^m}. \quad (21)$$

The H^m functions are given by

$$[H^m(\mu)]^{-1}=(1-\mu)^{-m}\prod_{j=1}^{m}1+(\mu/\nu_j{}^m)\times\exp\left((2\pi i)^{-1}\int_0^1\ln\frac{\Delta_+{}^m(\nu)}{\Delta_-{}^m(\nu)}[(\nu+\mu)^{-1}-\nu^{-1}]\,d\nu\right). \quad (22)$$

The $B^m(\nu,\mu)$ are given by

$$B^m(\nu,\mu)=\sum_{l=m}^{N-1}B_l{}^m(\nu)P_l{}^m(\mu), \quad (23)$$

where the $B_l{}^m$ are determined by solving the polynomial

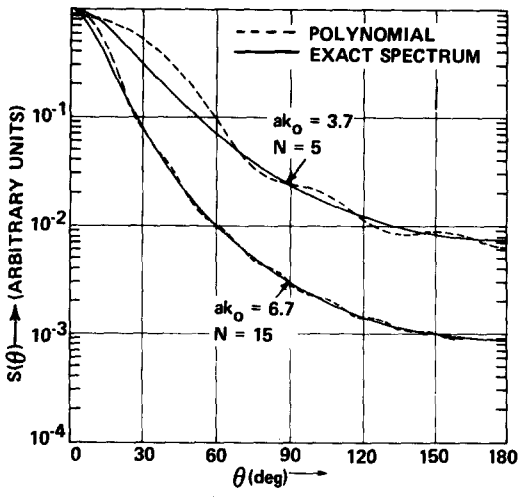

FIG. 2. Polynomial fits to von Kármán interpolation formula.

equations

$$\sum_{l=m}^{N-1} B_l^m(\nu') K_l^m(\nu) = -L^m(\nu, \nu'), \tag{24}$$

$$L^m(z, z') = (z-z')^{-1} \sum_{l=m}^{N} c_l^m \times [g_l^m(z) K_l^m(z') - g_l^m(z') K_l^m(z)], \tag{25}$$

$$K_l^m(\nu) = \int_0^1 p_l^m(\mu) \frac{[g^m(\nu, \mu) - g^m(\mu, \mu)]}{(\nu-\mu)} \mu H^m(\mu)\, dm(\mu) + 2\left[\frac{p_l^m(\nu)}{H^m(-\nu)}\right]_{AS}, \tag{26}$$

where AS means we keep the polynomial part in an expansion about $\nu = \infty$.

With the above results, we can write the final result as

$$I(x, \mu, \varphi) = \sum_{m=0}^{N} (2-\delta_{0,m}) I^m(x, \mu) (1-\mu^2)^{m/2} (1-\mu_0^2)^{m/2} \times \cos m(\varphi-\varphi_0) + \delta(\mu-\mu_0) \exp(-x/\mu_0) \times [\delta(\varphi-\varphi_0) - (2\pi)^{-1} \sum_{m=0}^{N} (2-\delta_{0,m}) \cos m(\varphi-\varphi_0)], \tag{27}$$

where (μ_0, φ_0) specify the incident wave direction.

C. Relation to Experimentally Measured Quantities

In order to calculate the intensity distribution given by Eq. (27) we need explicit expressions for the scattering phase function, the scattering per unit length σ, and the absorption per unit length κ. For the absorption per unit length, we use the development of Sen and Wyler[17] specialized to the case of small ν/ω,

$$\kappa = \nu \bar{N} / c N_{CR}, \tag{28}$$

where $\bar{N}$ is the mean plasma concentration, ν is the collision frequency, ω is the microwave frequency, N_{CR} is the critical plasma concentration, and c is the speed of light. For the scattering law, we assume that the criteria discussed by Watson[8] are satisfied. Then, the scattering law is simply given by the Born cross section

$$\sigma_{Born} = \sigma(\mathbf{r}) p(n, n') / 4\pi = r_e N_{rms}^2 S(\mathbf{k}-\mathbf{k}'), \tag{29}$$

where S is the spectral function of the electron density fluctuations, $\mathbf{k}$ and $\mathbf{k}'$ are the incident and scattered wave vectors, respectively, r_e is the classical electron radius, and N_{rms} is the root mean square of the electron density fluctuations. The scattering phase function is normalized such that

$$(4\pi)^{-1} \int p(n, n')\, d\Omega(n') = 1, \tag{30}$$

where $d\Omega(n')$ is a differential solid angle about n'. For the spectral function we assume the turbulence is isotropic and given by the von Kármán interpolation formula[18]

$$S(k) = Ca^3/(1+a^2k^2)^{11/6}, \tag{31}$$

where C is the normalization chosen to satisfy Eq. (30), a is the scale size that characterizes the spectrum, and k is the wave number. Because S depends only on the magnitude of $\mathbf{k}-\mathbf{k}'$, the scattering law is rotationally invariant.

It is also necessary to have a finite polynomial approximation of Eq. (31) in order to use the analysis as developed in McCormick and Kuščer.[12] In Fig. 2 we depict spectra and their polynomial approximations for two values of the product ak_0, where k_0 is the incident wavenumber. It is this product that governs the degree of anisotropy. The polynomial fits were chosen to both minimize the order and yield the correct ratio of forward to backscatter. We note that Watson has presented calculations for the isotropic case of $ak_0 = 0$.[9] The scattering angle θ is related to the wave number by

$$k = 2k_0 \sin\tfrac{1}{2}\theta.$$

Table I summarizes the various values of ak_0 used in the calculations. The value $ak_0 = 6.8$ approximately represents the degree of anisotropy for the axial spectral function and microwave wave length reported by Feinstein and Granatstein.[1] It is advantageous to use the lowest-order polynomial possible, since numerical calculations become progressively more difficult as the order is increased. Unfortunately, as the degree of anisotropy increases the order of the polynomial must be increased to obtain an adequate representation.

III. NUMERICAL RESULTS AND INTERPRETATION

The calculations (see Butler *et al.*[19] for a complete description), although quite involved, are actually reasonably straightforward. For example, considerable care must be taken to evaluate both the discrete roots

and integrands entering into the calculations. As roots appear at $\nu=1$, the integrands vary quite rapidly near $\mu=1$, and much finer grid spacing is required for evaluation of the integral in this region. In addition, calculations are difficult for large values of the discrete roots ν_j^m, because of the polynomial expansions used. The magnitude of ν_j^m increases with $\tilde{\omega}_0$, the single scatter albedo or ratio of scattering to total attenuation. Additional roots, ν_k^m, appear as the degree of anisotropy is increased. Hence, the calculations become more difficult as the scattering becomes more anisotropic or as $\tilde{\omega}_0$ approaches unity.

In Fig. 3 we show the root trajectories (ν_j^m vs $\tilde{\omega}_0$) for $ak_0=5.5$ or a ratio of forward to backscatter of 532.9 to 1. Since the roots ν_j^m are in the interval $(1, \infty)$, we have plotted (ν_j^m-1) to show their behavior near 1. The behavior for other ak_0 is, in general, the same. We observe that there is at least one root for $m=0$.[11] Additional roots appear for $m=0$ as $\tilde{\omega}_0$ increases and also for $m>0$.

TABLE I. Spectra used in calculations.

ak_0	Ratio of forward to backscatter	Order of polynomial
0	1	0
2.6	44.6	3
3.7	136.5	5
5.5	532.9	9
6.8	1143.3	15

All the roots reach an asymptotic value as $\tilde{\omega}_0$ approaches 1 except for the first root for $m=0$ which tends to infinity. It is this large magnitude which causes the computational problems. It is also this root which dominates the decay of the intensity for large optical depths. However, this root affects only the azimuthally independent part of the computation and thus the developments of Kaper *et al.*[15] and Eccleston *et al.*[20] may be used to overcome the numerical difficulties. Note, that although the scattering law is assumed azimuthally symmetric, neither the boundary conditions nor intensity distribution need be azimuthally symmetric.

Although computational time is not excessive, the numerical codes are quite involved, hence some verification of the calculations is desirable. Before discussing the intensity distribution calculations, let us briefly mention several such checks which have been made. Chandrasekhar[13] uses the discrete ordinate technique to solve the problem of reflection from a homogeneous half-space for an isotropic, linear, and quadratic (Rayleigh) scattering phase function. The present singular eigenfunction computation reproduces Chandrasekhar's results to the five figure accuracy he has published. As an additional check, one can show from

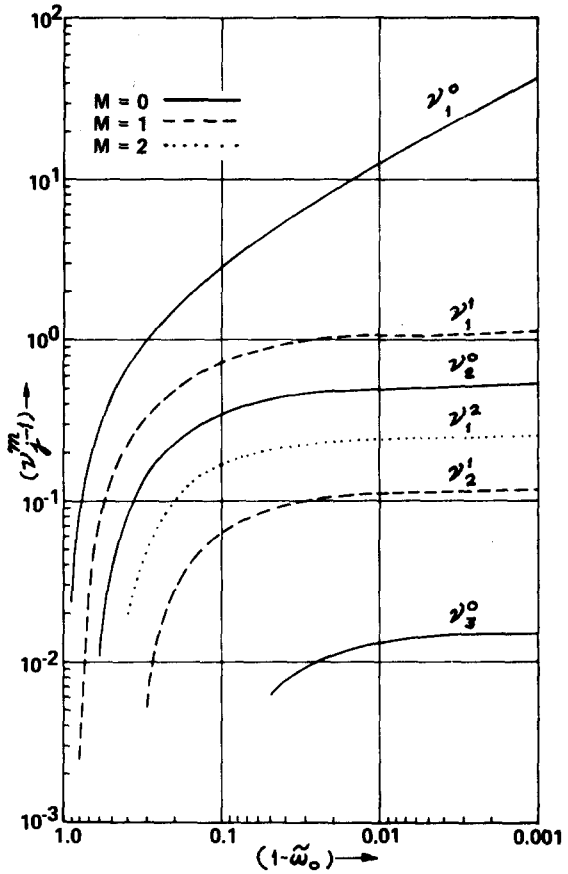

FIG. 3. Root trajectories for ratio of forward peaking of 532.9 to 1 with 9th order polynomial for $ak_0=5.5$.

the reciprocity relationship[12] that the eigenfunctions obey the following symmetry law

$$\mu_0\tilde{\phi}^m(-\mu, \mu_0)=\mu\tilde{\phi}^m(-\mu_0, \mu). \tag{32}$$

This relationship is satisfied for ratios of forward peaking up to at least 43.3 to 1 or $ak_0=6.8$.

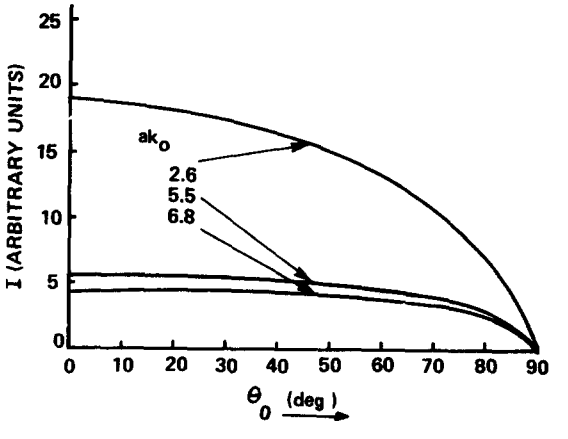

FIG. 4. Backscattered intensity from the half-space into the incident direction ($\theta=\pi-\theta_0$, $\varphi=\pi=\varphi_0$) as a function of incident direction.

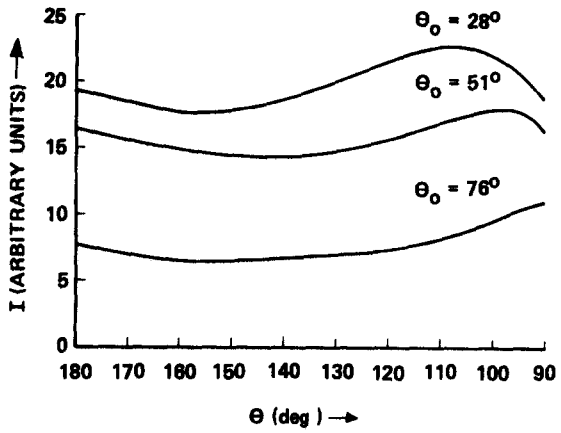

FIG. 5. Reflection from half-space for $ak_0=2.6$.

In Fig. 4 we display the backscattered intensity (i.e., $\mu=-\mu$, $\varphi=\pi+\varphi_0$. Hence, $\theta=\pi$ corresponds to intensity returning normal to the medium surface) for a forward peaking of 44.6 to 1 ($N=3$, $ak_0=2.6$), a forward peaking of 532.9 to 1 ($N=9$, $ak_0=5.5$), and a forward peaking of 1143.3 to 1 ($N=15$, $ak_0=6.8$), as a function of the incident directions for $\tilde{\omega}_0=0.7$. We note that the backscattered intensity is relatively insensitive to variations in the incident direction except near grazing incidence ($\theta=\pi/2$). The sensitivity is diminished as the forward peaking of the scattering function is increased, or equivalently as ak_0 is increased. We also observe that the backscattered intensity is larger for the less strongly peaked scattering functions or smaller ak_0. This result can be explained by the fact that, for the more strongly peaked scattering function the probability for backscatter is decreased. This leads to a longer pathlength in the medium and more energy will be lost by absorption. We have not included the special backscatter correction to the transport equation[8,9] which should affect the absolute magnitude but not the form of the curves.

In Figs. 5, 6, and 7 we present reflected intensity distributions for various incident angles for $ak_0=2.6$, 5.5, and 6.8, respectively, for $\tilde{\omega}_0=0.7$. We again observe the reduction in intensity as the scattering function becomes more strongly peaked. For $ak_0=2.6$, we observe maxima and minima as a function of θ. This behavior is also observed by Chandrasekhar[13] for low order polynomial scattering laws. The results for the higher-order fits shown in Figs. 6 and 7 still exhibit the extrema, but the amplitudes of the extrema are not nearly as large, indicating that the intensity reflected from the half space for a highly forward peaked scattering function is more diffuse, and relatively insensitive to angle of incidence. These results differ from the first order Born approximation which predicts a monotonic behavior for the bistatic backscattered intensity. We also note that, for all three scattering laws, the reflected intensity tends to reach a maximum and then decrease as θ approaches $\pi/2$ except for near grazing incidence. This phenomenon is also observed by Kaper *et al.*[15] in their eigenfunction solution for the slab with an azimuthally symmetric boundary condition. It may be understood if we consider a photon at an optical depth x in the medium traveling in direction μ toward the surface. The photon has an escape probability of $\exp(-x/\mu)$. As $\mu\to 0$ this probability decreases, decreasing the reflected intensity in this direction. This is analogous to limb darkening.

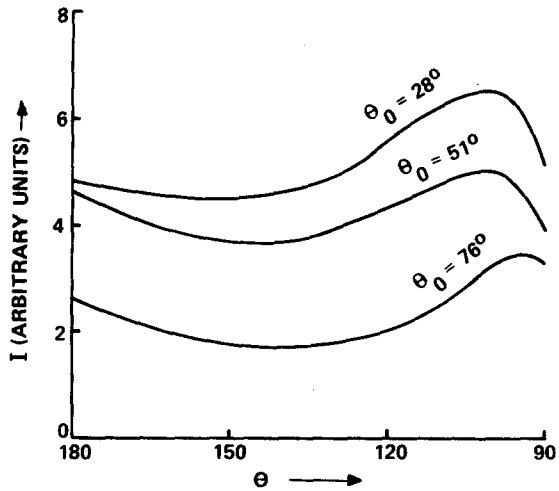

FIG. 7. Reflection from half-space for $ak_0=6.8$.

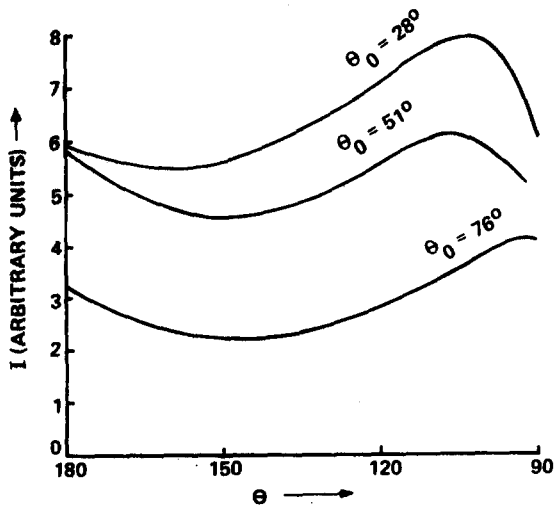

FIG. 6. Reflection from half-space for $ak_0=5.5$.

In Figs. 8 and 9 we show the radiance distribution as a function of optical depth for optical depths from 1 to 12, for a plane wave incident at 60° from the surface normal, for $\tilde{\omega}_0=0.7$. In Fig. 8 the ratio of forward

peaking is 136.5 to 1, and in Fig. 9 the ratio is 532.9 to 1. The curves represent only the scattered intensity at $\varphi=\varphi_0$, i.e., in the plane of the zenith and the incident directions. The unscattered intensity is a decaying exponential in x at $\theta=60°$. As expected for small optical depths, a maximum occurs about the incident direction. At greater depths in the medium, this maximum moves toward 0°, and the intensity distribution becomes independent of the angle of incidence. Comparing Figs. 8 and 9, we see that the observed maximum becomes more pronounced for a given depth as the scattering law becomes more strongly peaked in the forward direction, and one must go to larger optical depths before it

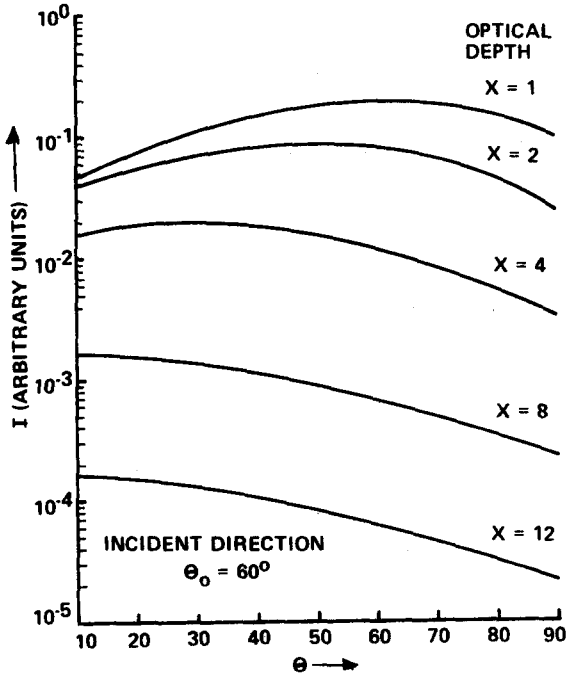

FIG. 8. Intensity distribution within the medium as a function of polar angle in plane of the zenith for $ak_0=3.7$.

diffuses. The rate of measured decay of the maximum about the incident angle, coupled with the ability to compute decay as a function of degree of forward peaking, may offer an indirect measure of this peaking and yield information about the spectrum.

The shift of the maximum to zero degrees is in agreement with the observations of underwater illumination in the sea.[21] The general structure of the intensity curves of Figs. 8 and 9 is also in qualitative agreement with such experimental data, e.g., that of Tyler.[22,23]

Figure 10 represents the same physical situation as Fig. 9, except we vary the optical depth x from 0.01 to 1.4. We observe that the peak about the incident direction disappears as the optical depth approaches zero, with a sharp maximum in the intensity occurring at 90° or parallel to the surface of the medium. One

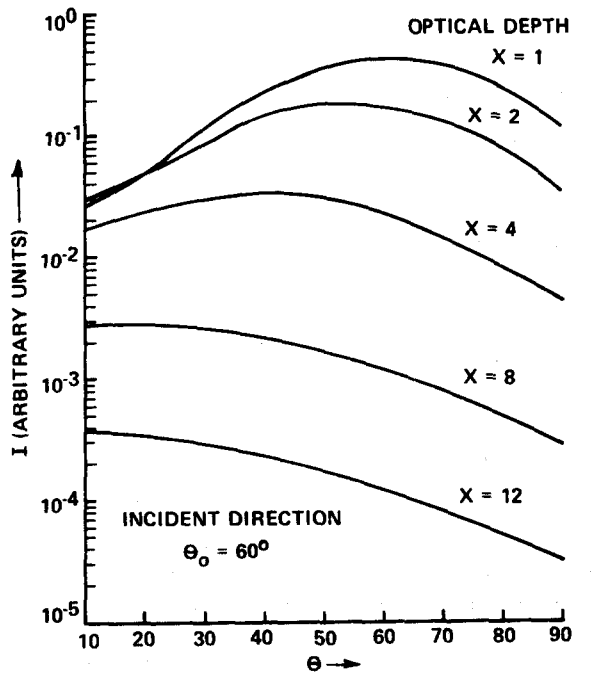

FIG. 9. Intensity distribution within the medium as a function of polar angle in plane of the zenith $ak_0=5.5$.

may think of this effect as photons trapped close to the surface, traveling parallel to the surface which is the reverse of the limb darkening effect described before. This phenomenon is observed by Tyler[22,23] in his underwater optics work. For the radiance at 0°, he first observes an increase then a decrease as the optical depth is increased which is in agreement with our calculations. Tyler also observes the maximum in the radiance dis-

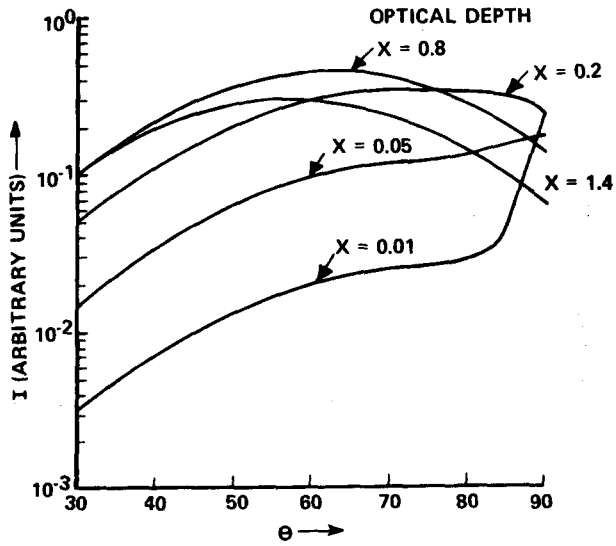

FIG. 10. Intensity distribution within the medium as a function of polar angle in plane of the zenith for small optical depths.

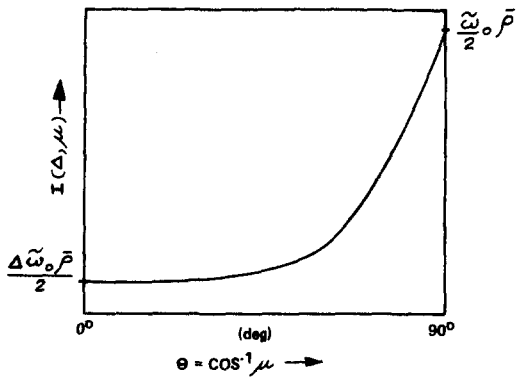

FIG. 11. Intensity distribution for isotropic scattering for small optical depths.

tribution shifting toward 90° as the optical depth approaches zero.

Both the photon trapping and limb darkening are not predicted by the Born approximation. One can, however, gain some insight into this behavior by looking at the case of isotropic scattering. We write the transport equation in the form

$$\left(\mu\frac{\partial}{\partial x}+1\right)I(x,\mu)=\tfrac{1}{2}(\tilde{\omega}_0)\rho(x), \tag{33}$$

where $\rho(x)$ is the integrated angular intensity

$$\rho(x)=\int_{-1}^{+1}I(x,\mu)\,d\mu. \tag{34}$$

The boundary condition is

$$I(0,\mu)=\delta(\mu-\mu_0), \qquad \mu>0. \tag{35}$$

The details of the solution to Eq. (33) can be found in the literature.[7] Here, we restrict our attention to small x.

We note immediately that if the derivative $(\partial/\partial x)\times I(x,\mu)$ is finite as $\mu\rightarrow 0$ then directly from Eq. (33) we have

$$I(x,0)=\tfrac{1}{2}\tilde{\omega}_0\rho(x). \tag{36}$$

To obtain the behavior for small $x\equiv\Delta$ we integrate the transport equation (33) and make use of the boundary condition Eq. (35),

$$I(\Delta,\mu)=\mu^{-1}\int_0^{\Delta}\exp\left(-\frac{\Delta-x'}{\mu}\right)\tfrac{1}{2}\tilde{\omega}_0\rho(x')\,dx' +\exp\left(-\frac{\Delta}{\mu}\right)\delta(\mu-\mu_0). \tag{37}$$

By the mean value theorem we can write

$$I(\Delta,\mu)=\tfrac{1}{2}\tilde{\omega}_0\frac{\bar{\rho}}{\mu}\int_0^{\Delta}\exp\left(-\frac{\Delta-x'}{\mu}\right)dx' +\exp\left(-\frac{\Delta}{\mu}\right)\delta(\mu-\mu_0), \tag{38}$$

where $\bar{\rho}$ is the value of $\rho(x)$ for some $0\leq x\leq\Delta$. Note that for small Δ, $\bar{\rho}$ will be close to $\rho(0)$. Equation (38) may be integrated to give

$$I(\Delta,\mu)=\tfrac{1}{2}\omega_0\bar{\rho}\left[1-\exp\left(-\frac{\Delta}{\mu}\right)\right] +\exp\left(-\frac{\Delta}{\mu}\right)\delta(\mu-\mu_0). \tag{39}$$

Now for small Δ/μ or $\mu\rightarrow 1$ we have

$$I(\Delta,\mu)\simeq\tfrac{1}{2}\tilde{\omega}_0\bar{\rho}\frac{\Delta}{\mu}+\exp\left(-\frac{\Delta}{\mu}\right)\delta(\mu-\mu_0). \tag{40}$$

For large Δ/μ or $\mu\rightarrow 0$ we have

$$I(\Delta,\mu)\simeq\tfrac{1}{2}\tilde{\omega}_0\bar{\rho}+\exp\left(-\frac{\Delta}{\mu}\right)\delta(\mu-\mu_0). \tag{41}$$

This behavior is shown in Fig. 11 where we have plotted only the collided intensity (omitting the delta function term). We observe that the behavior for the isotropic case is qualitatively the same as that for the full anisotropic calculation shown in Fig. 10 for $\Delta=0.1$.

Determination of electron concentration or collision frequency from a measurement of the reflected intensity, within the context of the present analysis, would require the single scatter albedo as a function of the reflected intensity. This is done in Fig. 12 for several different values ak_0 for normal backscatter. The first-order term in an $\tilde{\omega}_0$ expansion is also shown. We observe that there are significant departures from the first order approximation as the intensity is increased. We also observe a saturation effect, since $\tilde{\omega}_0$ cannot become greater than unity. In addition, we see that as the ak_0 is increased the curves rise more rapidly and saturate more sharply.

It has been observed experimentally[1,3,24,25] that the single scatter or modified first Born approximation seems to have wider range of applicability than origin-

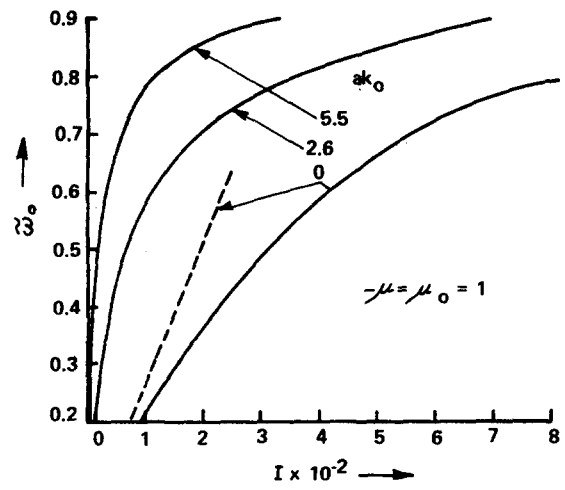

FIG. 12. Albedo as a function of normal backscattered intensity.

ally anticipated. In some of our earlier work with the Neumann series or multiple scatter expansion of the transport equation we have found that the second term of the solution contributes to the total solution in a manner to give an effective modified first Born appearance.[1,3] Perhaps some insight into this behavior may be gained by looking at the multiple scatter expansion for I

$$I=\sum_{n=1}^{\infty}\tilde{\omega}_0{}^n I_n \tag{42}$$

and then looking at the reciprocal relationship between $1/\tilde{\omega}_0$ and $1/I$.[26] Equation (42) is the Neumann series solution to the transport equation. Convergence is assured if $(I_{n+1}/I_n)<1/\tilde{\omega}_0$. It is important to realize that the series in Eq. (42) is not the same as the Born series solution to Maxwell's equations but rather an expansion in terms of the single scatter albedo $\tilde{\omega}_0$. However, the first term of the series in Eq. (42), I_1, is the well-known distorted wave Born approximation.[9] The utility of this approach is that one can obtain useful information about the general behavior of the solution without performing the lengthy numerical integrations necessary to calculate the I_n.

Before proceeding, we note from Eqs. (4), (29), and (31) that one cannot, in general, vary $\tilde{\omega}_0$ and ak_0 independently but, in the interpretation of the importance of multiple scatter, it is useful to consider the expansion in Eq. (42) for various ak_0.

From Eq. (42) we see immediately that for small $\tilde{\omega}_0$ we have the linear relation

$$I^{-1}\approx\tilde{\omega}_0{}^{-1}I_1{}^{-1}, \tag{43}$$

a straight line through the origin with slope $1/I_1$. The next order correction to Eq. (43) may be found by keeping terms to second order in $\tilde{\omega}_0$ in Eq. (42):

$$I^{-1}=(\tilde{\omega}_0 I_1)^{-1}[1+\tilde{\omega}_0(I_2/I_1)]^{-1}. \tag{44}$$

Hence, this correction is approximately

$$[1+\tilde{\omega}_0(I_2/I_1)]^{-1}\approx 1-\tilde{\omega}_0(I_2/I_1). \tag{45}$$

Equation (45) shows that the second-order term reduces the curve from the linear value; more for larger values of $\tilde{\omega}_0$ or smaller values of $1/\tilde{\omega}_0$. Combining Eqs. (44) and (45) gives

$$I^{-1}=(\tilde{\omega}_0 I_1)^{-1}-[I_2/(I_1)^2] \tag{46}$$

which shows that $1/I$ is linear in $1/\tilde{\omega}_0$ for small $\tilde{\omega}_0$.

In Fig. 13 we plot $1/I$ as a function of $1/\tilde{\omega}_0$ for several ratios of forward peaking for backscatter normal to the surface of the half-space ($\mu=-\mu_0=-1$). We observe that the linear relation predicted by the first- and second-order theory is obtained for the exact solution to the transport equation over a wide range of $\tilde{\omega}_0$. Slight deviations from linearity are observed as $\tilde{\omega}_0$ approaches 1. Here, the slope of the curve $1/I$ vs $1/\tilde{\omega}_0$ first decreases, behavior opposite to that predicted by Eq. (44). It was found numerically that further increases in $\tilde{\omega}_0$, although not apparent in Fig. 13, cause the slope to increase in agreement with Eq. (44). These transport equation calculations have been experimentally verified for scattering from a known spherical polydispersion[27] and have been compared with experimental measurements of underwater irradiance.[28]

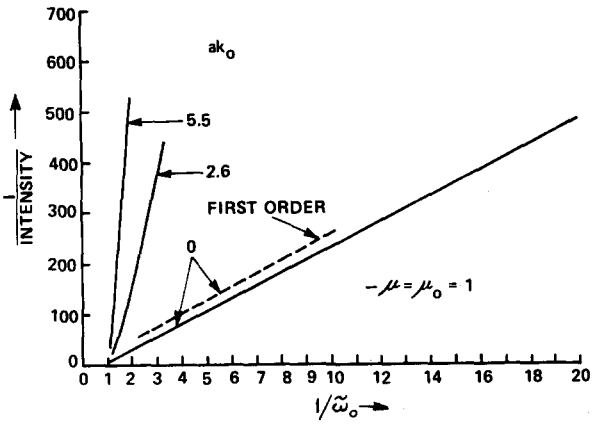

FIG. 13. Relationship between reciprocals of intensity and albedo.

We also observe that as the scattering law becomes more peaked in the forward direction (ak_0 is increased) the slope of the linear relation between $1/I$ and $1/\tilde{\omega}_0$ increases. This may be explained by the same argument used in the discussion of Fig. 4. For the more strongly peaked function of photon must, on the average, undergo many more scatterings, mostly through small angles, before it is emitted in the backscattered direction and, since its optical path in the medium is longer, more energy is lost to absorption. Hence, for a given $\tilde{\omega}_0$ or $1/\tilde{\omega}_0$, I will be smaller and $1/I$ larger as seen in Fig. 14.

The first-order approximation, Eq. (43), for isotropic scattering is also shown in Fig. 13. As expected the slope is the same as the exact calculation but the intercept is larger since the first-order approximation underestimates the exact solution.

In Fig. 14 we show the reciprocal relationships between $1/I$ and $1/\tilde{\omega}_0$ for several different backscatter and bistatic angles assuming isotropic scattering. We observe that the general linear relationship is still found over a wide range of parameters. We also observe that the slope is a function of the bistatic angle. The sensitivity of this dependence increases with the degree of anisotropy of the scattering law, hence may offer a method of probing the spectrum of turbulence.

An estimate of the full correction may be found by assuming that the ratio of successive terms approaches a constant

$$I_{n+1}/I_n\sim K\leq 1. \tag{47}$$

Mullikan,[29] in fact, has shown that for isotropic scat-

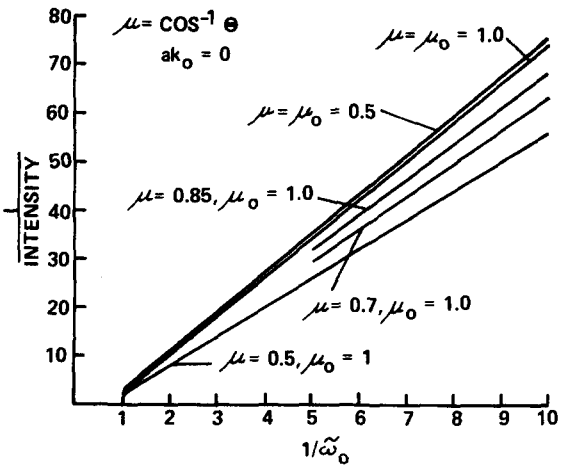

FIG. 14. Relationship between reciprocals of intensity and albedo for isotropic scattering for various angles.

tering and a half space medium

$$I_n \rightarrow \frac{\text{const}}{(n+1)^{3/2}}, \tag{48}$$

hence Eq. (47) holds exactly in the limit of large n. If we assume Eq. (47) holds to rather low order, say $n=2$, we have

$$I = \tilde{\omega}_0 I_1 [1 + \tilde{\omega}_0 (I_2/I_1)(1-\tilde{\omega}K)^{-1}], \tag{49}$$

where we have summed the geometric series in $\tilde{\omega}_0 K$. The reciprocal relation is

$$I^{-1} = (\tilde{\omega}_0 I_1)^{-1} \left[\frac{1-\tilde{\omega}_0 K}{1+\tilde{\omega}_0 [(I_2/I_1) - K]} \right]. \tag{50}$$

To second order in $\tilde{\omega}_0$ this is

$$I^{-1} = (\tilde{\omega}_0 I_1)^{-1} (I_2/I_1^2) + \tilde{\omega}_0 (K/I_1)[(I_2/I_1) - K]. \tag{51}$$

The first two terms of Eq. (51) are identical to Eq. (46). The deviation from the linear relationship is given by the third term. The precise form of the deviation depends on the magnitudes of I_1, I_2, and K. Note that if we had taken $n=1$ in Eq. (47), then Eq. (51) would reduce to the linear relationship, Eq. (46).

To better understand these results we can analytically perform exact calculations for the case of isotropic scattering. For the ratio I_2/I_1, we obtain, for the exact solution $I_2/I_1 = 0.693$, and from Eq. (48), $I_2/I_1 = 0.649$; hence, we see that taking $K=1$ for low n is an overestimate. The effect of these approximations may be seen in Fig. 15 where for isotropic scattering we have plotted the first-order term, Eq. (43), the linear approximation, Eq. (46), Eq. (50) with $K=1$ for $n \geq 2$, and the exact solution. We see all four curves are approximately linear over the range of $\tilde{\omega}_0$ calculated $(0.1 \leq \tilde{\omega}_0 \leq 0.9)$. It is interesting to note that the linear approximation, Eq. (46), does not significantly improve the first-order result, Eq. (43). However, the additional higher-order terms approximated in Eq. (50) do show substantial improvement. We have thus demonstrated analytically and numerically, for the case of isotropic scattering, that the higher order terms contribute to $1/I$ in a manner that yields a slope equal to $(\tilde{\omega}_0 I_1)^{-1}$, over a wide range of $\tilde{\omega}_0$ $(0.1 \leq \tilde{\omega}_0 < 0.9)$.

Finally, it should be pointed out that, although no mention of the "saturation" effect discussed in the literature[1,14,24] has been made, this effect is a natural consequence of the transport solution. The exponential nature of the expansion, Eq. (16) explicitly shows this effect. In fact, as the scattering becomes strong (i.e., $\tilde{\omega}_0 \sim 1$) the first root ν_1^0 dominates as is shown in Fig. 3 and saturation occurs.

IV. SUMMARY

We have formulated the problem of electromagnetic scattering in a turbulent plasma in terms of the radiative transport equation. A singular eigenfunction solution was given for the case of an azimuthally symmetric scattering law, i.e., for scattering by typical homogeneous isotropic plasma turbulence. The degree of anisotropy in the scattering function is governed by the product of the turbulent scale size and the wave number of the incident electromagnetic wave.

Detailed numerical calculations were presented based on a finite polynomial approximation to the turbulent spectrum. The intensity distribution was studied as a function of angle and depth in the turbulent medium. The effects of varying the scattering albedo and the turbulent spectrum were also studied. Several interesting phenomena were found to be present including limb darkening, photon trapping near the surface, and an approximate linear relation between the reciprocals of intensity and albedo.

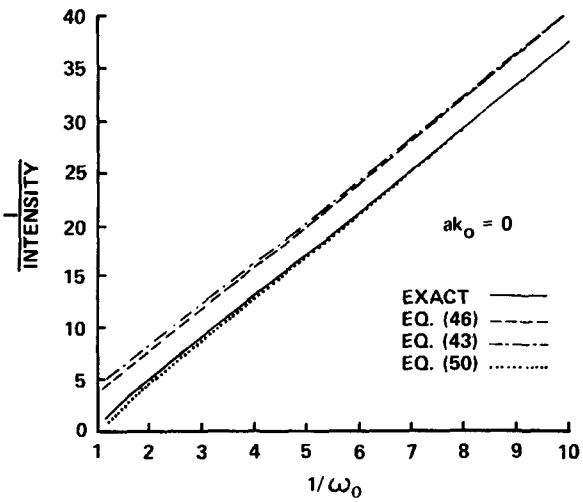

FIG. 15. Relationship between reciprocals of intensity and albedo for isotropic scattering.

In order to make direct comparisons with experiment, the solutions must be modified to consider the effects of inhomogenities, finite geometries, and anisotropic plasma turbulence.

ACKNOWLEDGMENTS

The authors would like to express their gratitude to the many people who contributed to this work. In particular we wish to thank J. T. Fleck of the Cornell Aeronautical Laboratory and N. J. McCormick of the University of Washington for their suggestions in helping to overcome the computational difficulties. We also want to thank T. O. Philips and A. M. Levine of Bell Telephone Laboratories and S. N. Samaddar and K. R. Edwards of the Cornell Aeronautical Laboratory with whom we had many instructive discussions on the interpretation of the results.

This work was supported by Cornell Aeronautical Laboratory Internal Research funds.

* Present address: Department of Mathematics, University of Wisconsin, River Falls, Wisconsin 54022.

[1] D. L. Feinstein and V. L. Granatstein, Phys. Fluids **12**, 2658 (1969).

[2] D. L. Feinstein and V. L. Granatstein, Bull. Am. Phys. Soc. **14**, 582 (1969).

[3] D. L. Feinstein and V. L. Granatstein, Bull. Am. Phys. Soc. **15**, 1414 (1970).

[4] Yu. A. Shreider, *The Monte Carlo Method* (Pergamon, New York, 1966), p. 137.

[5] R. Bellman in *Transport Theory*, edited by R. Bellman, G. Birkhoff, and I. Abu-Shumays (American Mathematical Society, Providence, R. I., 1969), Vol. 1, p. 95.

[6] E. M. Gelbard, J. A. Davis, and L. A. Hageman in *Transport Theory*, edited by R. Bellman, G. Birkhoff, and I. Abu-Shumays (American Mathematical Society, Providence, R.I., 1969), Vol. 1, p. 129.

[7] K. M. Case and P. F. Zweifel, *Linear Transport Theory* (Addison-Wesley, Reading, Mass. 1967).

[8] K. M. Watson, J. Math. Phys. **10**, 688 (1969).

[9] K. M. Watson, Phys. Fluids **13**, 2514 (1970).

[10] P. E. Scott, J. Phys. A. **1**, 675 (1968).

[11] J. R. Mika, Nucl. Sci. Eng. **11**, 415 (1961).

[12] N. J. McCormick and I. Kuščer, J. Math. Phys. **7**, 2036 (1966).

[13] S. Chandrasekhar, *Radiative Transfer* (Dover, New York, 1960).

[14] I. P. Shkarofsky, Radio Sci. (to be published).

[15] H. G. Kaper, J. K. Shultis, and J. G. Veninga, J. Comp. Phys. **6**, 288 (1970).

[16] W. M. Irvine, Astrophys. J. **152**, 823 (1968).

[17] H. K. Sen and A. A. Wyler, J. Geophys. Res. **65**, 3931 (1960).

[18] V. I. Tatarski, *Wave Propagation in a Turbulent Medium* (Dover, New York, 1961), p. 7.

[19] F. E. Butler, D. L. Feinstein, K. R. Piech, and A. Leonard, Cornell Aeronautical Laboratory Report No. UB-1376-S-189, RMAR 70-9 (1970).

[20] G. W. Eccleston, Jr. and N. J. McCormick, J. Nucl. Energy **24**, 23 (1970).

[21] S. Q. Duntley, J. Opt. Soc. Am. **53**, 228 (1963).

[22] J. E. Tyler, Limnol. Oceanog. **6**, 451 (1961).

[23] J. E. Tyler, Bull. Scripps Inst. Oceanog. **1**, 363 (1960).

[24] H. Guthart and K. Graf, Radio Sci. **5**, 1099 (1970).

[25] C. Richard, A. K. Ghosh, and I. P. Shkarofsky, Phys. Fluids **14**, 398 (1971).

[26] We are indebted to Dr. A. M. Levine for his suggestion of this development.

[27] M. Rhinewine, A. M. Levine, V. L. Granststein, D. L. Feinstein, M. J. Mazurowski, and K. R. Piech, Appl. Opt. **11**, 1217 (1972).

[28] D. L. Feinstein, K. R. Piech, and A. Leonard, in *AGARD Conference Proceedings No. 77 on Electromagnetics of the Sea* (North Atlantic Treaty Organization, Paris, France, 1970), paper 38.

[29] T. W. Mullikin, United States Atomic Energy Commission, Division of Technical Information, ORO-3858-1, p. 121 (1969).